

Received January 14, 2020, accepted February 14, 2020, date of publication February 27, 2020, date of current version March 16, 2020.

Digital Object Identifier 10.1109/ACCESS.2020.2976503

Stability and Direction Control of a Two-Wheeled Robotic Wheelchair Through a Movable Mechanism

MOSTAFA NIKPOUR^{id}, LOULIN HUANG^{id}, (Member, IEEE), AND AHMED M. AL-JUMAILY^{id}

Institute of Biomedical Technologies, Auckland University of Technology, Auckland 1010, New Zealand

Corresponding author: Loulin Huang (loulin.huang@aut.ac.nz)

ABSTRACT A two-wheeled robotic wheelchair (TWRW) has a better manoeuvrability than a conventional four-wheeled wheelchair. However, it is not statically stable near the upright posture or a posture desired by the rider, and an active stability controller is required. Stability control becomes more challenging when a TWRW is also required to move in a desired direction. To rely on wheels' motions to achieve both stability and direction control tend to impose a large burden on the wheels' driving motors or other types of actuators in terms of their driving torque and power consumption. Various disturbances in the system also affect the performance of the controller. To solve these problems, this paper presents a stability and direction controller based on the motion of a pendulum-like movable mechanism added to assist the wheels to produce control actions. The dynamic model of the TWRW is established through the Euler-Lagrange formulation in which the disturbances caused by model uncertainties and rider's motion are considered. A robust second-order sliding mode control is then developed for the stability and the direction control of a TWRW. Simulation results are presented to validate the effectiveness of the proposed method.

INDEX TERMS Two-wheeled robotic wheelchair, stability control, direction control, added movable mechanism, second-order sliding mode control.

I. INTRODUCTION

A conventional robotic wheelchair consists of two driving wheels and two passive casters, where the driving wheels move actively for both mobility and stability of the wheelchair, while the passive casters provide a support for the wheelchair's stability [1]–[3]. A two-wheeled robotic wheelchair (TWRW) without casters can turn on spot, climb small steps, and thus has a better manoeuvrability than a conventional wheelchair [4]. It is also compact in structure and can maneuver in a narrow space [5].

However, a TWRW which can be modelled as a two-wheeled inverted pendulum, is not statically stable as a conventional wheelchair at the upright posture (defined by a pitch angle) and needs an active controller to be stabilized [6]. When a TWRW is also required to follow a path along a desired direction (defined by a yaw angle), to achieve both stability and direction control is more challenging. The TWRW is also subjected to disturbances caused by the unmodelled dynamics, rider's motion, sensor

noises and uneven surface, etc which affect the controller's performance [7], [8].

Different motion patterns of a TWRW such as turning, going straight or standing still are produced from the relative angular velocity between two driving wheels; this is called differential wheel drive mechanism [4], [9]–[12]. Such a mechanism has a high demand on torque and power consumption from the driving motors. Another approach for stability control is based on the motion of a movable seat or a linearly moving mass slider under the rider's seat [13], [14]. Though it needs less torque and power consumption for stability control, its operation range is limited, and it tends to cause unwanted disturbances affecting the comfort of the rider.

For a nonlinear system like a TWRW with different driving mechanisms, the common nonlinear controller *Computed Torque Control* can be applied for stability and direction control [15]. In this controller, the control inputs (torques) are derived from nonlinear state feedback and closed loop tracking errors through the system dynamic model. However, it requires an accurate dynamic model of the system and is not robust against model and external uncertainties [5]. In comparison, sliding mode control (SMC) is more robust against

The associate editor coordinating the review of this manuscript and approving it for publication was Nishant Unnikrishnan.

disturbances and is more computationally efficient [16]–[18]. In this controller, the closed loop tracking errors are forced to be near a predefined surface, called *sliding surface*, in the state space of the system. For an underactuated systems where the number of inputs is less than the number of controlled outputs, hierarchical sliding mode control (HSMC) can be applied [19]. In HSMC, the system is divided into several subsystems for each of which, a so called *layer sliding surface* is designed. The main drawback of SMC control is chattering phenomenon which leads to high vibration in the system. This problem can be solved with quasi-sliding mode control (QSMC) where a smooth sigmoid function is used to replace a non-smooth sign function found in a SMC controller [20]. Another effective solution is higher order sliding mode controller like the second order sliding mode controller (SOSMC) [21]. In this controller, a discontinuous integrator is added to the control input to eliminates the chattering phenomenon.

Both stability control and direction control of a TWRW are required in practice, but this issue has not been addressed in the existing research. A main challenging is to achieve the both control targets well when the system is subject to various disturbances and torques and power consumption are constrained by the limits of the wheel motors' capacities. In this paper, pendulum-like movable mechanism is added to the TWRW to assist the wheels for stability and direction control. The dynamic model of the system is established using Euler-Lagrange formulation. Disturbances from model uncertainties of system and rider's motion are also considered. A SOSMC is developed for stability and direction control of the TWRW. The proposed approach is shown to be superior conventional methods in terms of the performance of the controller and the control torque and power consumption needed.

The rest of paper is organized as follows. The TWRW is described and its dynamic model is derived in Sect. II. In Sect. III, a SOSMC for stability and direction control of the TWRW is presented. Simulation results to validate the effectiveness of the proposed control approach are presented and discussed in Sect. IV. Conclusions are given in Sect. V.

II. WHEELCHAIR MODELLING

A TWRW consists of two wheels and a seat for the rider which can rotate freely around the wheels axle; the seat and the rider are combined to form a body. A pendulum like movable mechanism is placed under the seat to assist the wheels to control the TWRW. This mechanism consists of a rod and a mass placed at one end of rod. The mass of rod is small and is neglected. Fig. 1 shows a prototype of a TWRW.

Fig. 2 shows the schematic view of the TWRW and the proposed mechanism. The nomenclature can be found in Table. 1. To derive the dynamic model of the TWRW, the Euler-Lagrange formulation is used, [22]

$$\frac{d}{dt} \left(\frac{\partial L}{\partial \dot{q}_i} \right) - \frac{\partial L}{\partial q_i} = Q_i \quad (1)$$



FIGURE 1. TWRW prototype.

where $L = T - U$ is known as Lagrangian and T and U are the kinetic and potential energy of the whole system, respectively. The system's generalized coordinates and their corresponding inputs are denoted by q_i and Q_i , respectively. The friction forces between joints are not considered. Also, it is assumed that the wheels don't slip on the ground. In conventional control method, the wheels torques are the control inputs. Therefore, the overall kinetic and potential energy of system can be obtained as

$$T = T_r + T_l + T_b, \quad U = U_r + U_l + U_b.$$

where T_r , T_l and T_b are the kinetic energy of right and left wheel and body (including rider and seat frame), respectively. Similarly, U_r , U_l and U_b are their potential energies. The kinetic energy of right and left wheel can be shown as

$$T_r = \frac{1}{2} m_w r^2 \dot{\theta}_r^2 + \frac{1}{2} J_{w_y} \dot{\theta}_y^2 + \frac{1}{2} J_{w_z} \dot{\theta}_r^2$$

$$T_l = \frac{1}{2} m_w r^2 \dot{\theta}_l^2 + \frac{1}{2} J_{w_y} \dot{\theta}_y^2 + \frac{1}{2} J_{w_z} \dot{\theta}_l^2$$

$\dot{\theta}_y$ which is the yaw angular velocity can be obtained as [23]

$$\dot{\theta}_y = \frac{r}{d} (\dot{\theta}_r - \dot{\theta}_l) \quad (2)$$

The kinetic energy of body can be obtained as

$$T_b = \frac{1}{2} m_b (V^2 + l^2 \dot{\theta}_b^2 + l^2 \dot{\theta}_y^2 \sin^2 \theta_b + 2Vl \dot{\theta}_b \cos \theta_b)$$

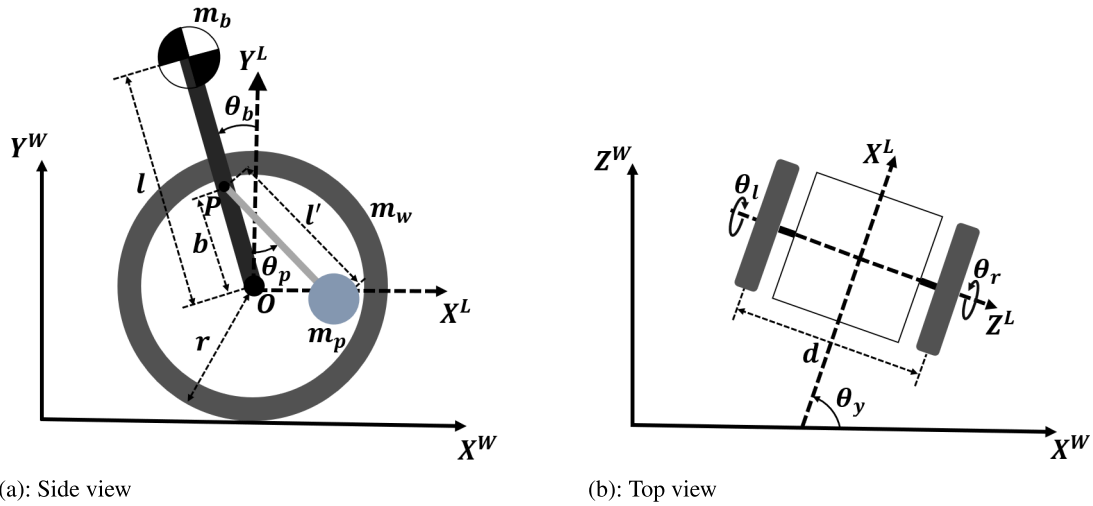
$$+ \frac{1}{2} (J_{b_x} \dot{\theta}_y^2 \sin^2 \theta_b + J_{b_y} \dot{\theta}_y^2 \cos^2 \theta_b + J_{b_z} \dot{\theta}_b^2)$$

where V is the linear velocity of center of wheels axle which is

$$V = \frac{r}{2} (\dot{\theta}_r + \dot{\theta}_l) \quad (3)$$

The potential energy of the right and left wheels and the body can be shown as

$$U_r = U_l = 0, \quad U_b = m_b g l \cos \theta_b.$$


FIGURE 2. Model of a two-wheeled wheelchair and proposed mechanism.
TABLE 1. Nomenclature.

Notation	Definition
$X^W - Y^W - Z^W$	World coordinate frame
$X^L - Y^L - Z^L$	TWRW coordinate frame attached to the middle of wheel axle
O	Middle of wheel axle
P	The point movable mechanism is added to the TWRW
θ_r, θ_l	Rotation angle of the right and left wheel measured from Y^L axis
θ_b	Rotation angle of the body (pitch angle) measured from Y^L axis
θ_p	Rotation angle of the added movable mechanism measured from link OP
θ_y	Yaw angle of the TWRW measured from X^W axis
m_w, m_b, m_p	Mass of each wheel, body and added mechanism, respectively
J_{w_y}, J_{w_z}	Moment of inertia of each wheel at their center of gravity (CoG) in wheel's local frame
$J_{b_x}, J_{b_y}, J_{b_z}$	Moment of inertia of body at its CoG in body's local frame
$J_{p_x}, J_{p_y}, J_{p_z}$	Moment of inertia of added mechanism at its CoG in added mechanism's local frame
r	Radius of each wheel
d	Length of wheels axle
l	Distance between the body's CoG and point O
l'	Length of the added mechanism's rod
b	Distance between point O and P
τ_r, τ_l, τ_p	Input torque of right and left wheels and added mechanism, respectively
P_r, P_l, P_p	Input power of right and left wheels and added mechanism motors, respectively
E_r, E_l, E_p	Energy consumption of right and left wheels and added mechanism motors, respectively

Applying Equation (1), the dynamic model of TWRW in the conventional method can be derived and presented as [24]

$$\mathbf{M}_c \ddot{\mathbf{q}}_c + \mathbf{H}_c + \mathbf{G}_c = \mathbf{B}_c \boldsymbol{\tau}_c \quad (4)$$

where \mathbf{q}_c is the generalized coordinates vector that can be shown as

$$\mathbf{q}_c = [\theta_r \quad \theta_l \quad \theta_b]^T$$

\mathbf{M}_c is the symmetric matrix called the inertia matrix.

$$\mathbf{M}_c = \begin{bmatrix} M_{c11} & M_{c12} & M_{c13} \\ M_{c21} & M_{c22} & M_{c23} \\ M_{c31} & M_{c32} & M_{c33} \end{bmatrix}$$

\mathbf{H}_c is the Centrifugal and Coriolis forces matrix.

$$\mathbf{H}_c = [H_{c1} \quad H_{c2} \quad H_{c3}]^T$$

\mathbf{M}_c and \mathbf{H}_c components can be found in Appendix A. \mathbf{G}_c is the gravity matrix.

$$\mathbf{G}_c = [0 \quad 0 \quad -m_b g l \sin \theta_b]^T$$

\mathbf{B}_c is the control coefficient matrix.

$$\mathbf{B}_c = \begin{bmatrix} 1 & 0 & 0 \\ 0 & 1 & 0 \end{bmatrix}^T$$

and $\boldsymbol{\tau}_c$ is the control input vector.

$$\boldsymbol{\tau}_c = [\tau_r \quad \tau_l]^T$$

The input power and energy consumption of right and left wheel motors can be obtained as [25]

$$P_r = \tau_r \dot{\theta}_r, \quad P_l = \tau_l \dot{\theta}_l, \quad E_r = \int P_r dt, \quad E_l = \int P_l dt.$$

Considering the disturbances like model uncertainties due to the varying mass of the rider and the variations of the body's center of gravity (CoG) from the motions of the rider, the dynamic model of system should be reformulated as

$$\hat{\mathbf{M}}_c \ddot{\mathbf{q}}_c + \hat{\mathbf{H}}_c + \hat{\mathbf{G}}_c + \mathbf{D}_c + \mathbf{R}_c = \mathbf{B}_c \boldsymbol{\tau}_c \quad (5)$$

where \mathbf{D}_c and \mathbf{R}_c denotes the disturbances caused by model uncertainties and change of body's CoG position, respectively. $\hat{\mathbf{M}}_c$, $\hat{\mathbf{H}}_c$ and $\hat{\mathbf{G}}_c$ are the nominal inertia, centrifugal and gravity matrices, respectively and can be shown as

$$\hat{\mathbf{M}}_c = \mathbf{M}_c - \Delta \mathbf{M}_c, \quad \hat{\mathbf{H}}_c = \mathbf{H}_c - \Delta \mathbf{H}_c, \quad \hat{\mathbf{G}}_c = \mathbf{G}_c - \Delta \mathbf{G}_c$$

The disturbance caused by the uncertain mass of the body can be shown as

$$\mathbf{D}_c = \Delta \mathbf{M}_c \ddot{\mathbf{q}}_c + \Delta \mathbf{H}_c + \Delta \mathbf{G}_c$$

where

$$\Delta \mathbf{M}_c = \begin{bmatrix} \Delta M_{11} & \Delta M_{12} & \Delta M_{13} \\ \Delta M_{21} & \Delta M_{22} & \Delta M_{23} \\ \Delta M_{31} & \Delta M_{32} & \Delta M_{33} \end{bmatrix}$$

$$\Delta \mathbf{H}_c = [\Delta H_1 \quad \Delta H_2 \quad \Delta H_3]^T$$

$$\Delta \mathbf{G}_c = [0 \quad 0 \quad -\Delta m_b g l \sin \theta_b]^T$$

$\Delta \mathbf{M}_c$ is a symmetric matrix. $\Delta \mathbf{M}_c$ and $\Delta \mathbf{H}_c$ components are shown in Appendix A. $\Delta m_b = m_b - \hat{m}_b$, where m_b and \hat{m}_b are the real and nominal values of body's mass, respectively.

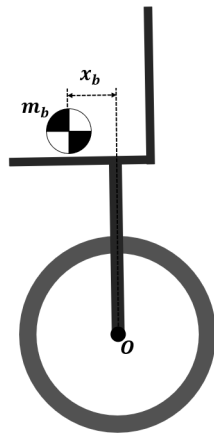


FIGURE 3. Change of body's CoG position.

The body's CoG varies when the rider moves on the seat. Assume its position along the forward direction is defined by x_b as shown in Fig. 3, the kinetic and potential energy of body are reformulated as

$$T_b = \frac{1}{2} m_b [V^2 + l^2 \dot{\theta}_b^2 + l^2 \dot{\theta}_y^2 \sin^2 \theta_b + 2Vl \dot{\theta}_b \cos \theta_b + x_b^2 \dot{\theta}_b^2 + x_b^2 \dot{\theta}_y^2 \cos^2 \theta_b + l x_b \dot{\theta}_y^2 \sin 2\theta_b - 2x_b V \dot{\theta}_b \sin \theta_b] + \frac{1}{2} (J_{b_x} \dot{\theta}_y^2 \sin^2 \theta_b + J_{b_y} \dot{\theta}_y^2 \cos^2 \theta_b + J_{b_z} \dot{\theta}_b^2 \cos^2 \theta_b),$$

$$U_b = m_b g (l \cos \theta_b + h \sin \theta_b).$$

The effect of change of body's CoG can be shown as

$$\mathbf{R}_c = [R_1 \quad R_2 \quad R_3]^T$$

The \mathbf{R}_c elements are shown in Appendix A. From Equation (5), we have

$$\ddot{\mathbf{q}}_c = \hat{\mathbf{M}}_c^{-1} (-\hat{\mathbf{H}}_c - \hat{\mathbf{G}}_c - \mathbf{D}_c - \mathbf{R}_c + \mathbf{B}_c \boldsymbol{\tau}_c) \quad (6)$$

Differentiating Equation (2), with respect to time leads to

$$\ddot{\theta}_y = \frac{r}{d} (\ddot{\theta}_r - \ddot{\theta}_l) \quad (7)$$

From Equation (6), and Equation (7), we have

$$\ddot{\theta}_b = A_{c1} + B_{c1} + \hat{M}_{c31}^{-1} \tau_r + \hat{M}_{c32}^{-1} \tau_l,$$

$$\ddot{\theta}_y = \frac{r}{d} [A_{c2} + B_{c2} + (\hat{M}_{c11}^{-1} - \hat{M}_{c21}^{-1}) \tau_r + (\hat{M}_{c12}^{-1} - \hat{M}_{c22}^{-1}) \tau_l]. \quad (8)$$

The definition of A_{c1} , B_{c1} , A_{c2} , and B_{c2} can be found in Appendix A.

Considering the added pendulum like movable mechanism, the overall kinetic and potential energy of TWRW is obtained as

$$T = T_r + T_l + T_b + T_p, \quad U = U_r + U_l + U_b + U_p.$$

where T_p and U_p are the kinetic and potential energy of the added movable mechanism, respectively. T_p and U_p can be presented as

$$T_p = \frac{1}{2} m_p [V^2 + b^2 \dot{\theta}_b^2 + 2bV \dot{\theta}_b \cos \theta_b + l'^2 (\dot{\theta}_b + \dot{\theta}_p)^2 - 2l'V (\dot{\theta}_b + \dot{\theta}_p) \cos (\theta_b + \theta_p) - 2bl' \dot{\theta}_b (\dot{\theta}_b + \dot{\theta}_p) \cos \theta_p + b^2 \dot{\theta}_y^2 \sin^2 \theta_b + l'^2 \dot{\theta}_y^2 \sin^2 (\theta_b + \theta_p) - 2bl' \dot{\theta}_y^2 \sin \theta_b \sin (\theta_b + \theta_p)] + \frac{1}{2} [J_{p_x} \dot{\theta}_y^2 \sin^2 (\theta_b + \theta_p) + J_{p_y} \dot{\theta}_y^2 \cos^2 (\theta_b + \theta_p) + J_{p_z} (\dot{\theta}_b + \dot{\theta}_p)^2],$$

$$U_p = m_p g (b \cos \theta_b - l' \cos (\theta_p + \theta_b)).$$

By applying Equation (1), the dynamic model of the whole system is as follows,

$$\mathbf{M}_p \ddot{\mathbf{q}}_p + \mathbf{H}_p + \mathbf{G}_p = \mathbf{B}_p \boldsymbol{\tau}_p \quad (9)$$

where

$$\mathbf{q}_p = [\theta_r \quad \theta_l \quad \theta_b \quad \theta_p]^T$$

$$\mathbf{M}_p = \begin{bmatrix} M_{p11} & M_{p12} & M_{p13} & M_{p14} \\ M_{p21} & M_{p22} & M_{p23} & M_{p24} \\ M_{p31} & M_{p32} & M_{p33} & M_{p34} \\ M_{p41} & M_{p42} & M_{p43} & M_{p44} \end{bmatrix}$$

$$\mathbf{G}_p = [0 \quad 0 \quad G_{p3} \quad G_{p4}]^T$$

$$\mathbf{B}_p = \begin{bmatrix} 1 & 0 & 0 & 0 \\ 0 & 1 & 0 & 0 \\ 0 & 0 & 0 & 1 \end{bmatrix}^T, \quad \boldsymbol{\tau}_p = [\tau_r \quad \tau_l \quad \tau_p]^T$$

\mathbf{M}_p , \mathbf{H}_p and \mathbf{G}_p components can be found in Appendix B. The input power and energy consumption of added movable mechanism motor can be obtained as [25]

$$P_p = \tau_p \dot{\theta}_p, \quad E_p = \int P_p dt.$$

Considering model uncertainties and change of body's CoG position, the dynamic model is rewritten as

$$\hat{\mathbf{M}}_p \ddot{\mathbf{q}}_p + \hat{\mathbf{H}}_p + \hat{\mathbf{G}}_p + \mathbf{D}_p + \mathbf{R}_p = \mathbf{B}_p \boldsymbol{\tau}_p \quad (10)$$

where

$$\begin{aligned} \mathbf{D}_p &= \Delta \mathbf{M}_p \ddot{\mathbf{q}}_p + \Delta \mathbf{H}_p + \Delta \mathbf{G}_p \\ \Delta \mathbf{M}_p &= \begin{bmatrix} \Delta M_{11} & \Delta M_{12} & \Delta M_{13} & 0 \\ \Delta M_{21} & \Delta M_{22} & \Delta M_{23} & 0 \\ \Delta M_{31} & \Delta M_{32} & \Delta M_{33} & 0 \\ 0 & 0 & 0 & 0 \end{bmatrix} \\ \Delta \mathbf{H}_p &= [\Delta H_1 \quad \Delta H_2 \quad \Delta H_3 \quad 0]^T \\ \Delta \mathbf{G}_p &= [0 \quad 0 \quad -\Delta m_b g l \sin \theta_b \quad 0]^T \\ \mathbf{R}_p &= [R_1 \quad R_2 \quad R_3 \quad 0]^T \end{aligned}$$

$\Delta \mathbf{M}_p$, $\Delta \mathbf{H}_p$ and \mathbf{R}_p elements are similar to the disturbances matrices derived in conventional method and can be found in Appendix A. In proposed method, $\ddot{\theta}_b$ and $\ddot{\theta}_y$ can be obtained as

$$\begin{aligned} \ddot{\theta}_b &= A_{p1} + B_{p1} + \hat{M}_{p31}^{-1} \tau_r + \hat{M}_{p32}^{-1} \tau_l + \hat{M}_{p34}^{-1} \tau_p, \\ \ddot{\theta}_y &= \frac{r}{d} [A_{p2} + B_{p2} + (\hat{M}_{p11}^{-1} - \hat{M}_{p21}^{-1}) \tau_r \\ &\quad + (\hat{M}_{p12}^{-1} - \hat{M}_{p22}^{-1}) \tau_l + (\hat{M}_{p14}^{-1} - \hat{M}_{p24}^{-1}) \tau_p]. \quad (11) \end{aligned}$$

The definition of A_{p1} , B_{p1} , A_{p2} , and B_{p2} are presented in Appendix B.

III. CONTROLLER DESIGN

A. CONVENTIONAL METHOD

The control objective is to track the desired yaw angle by the TWRW, while the pitch angle remains zero. To control the pitch and yaw angle through SOSMC, the sliding surface vector is defined as

$$\boldsymbol{\sigma} = [\sigma_1 \quad \sigma_2]^T, \quad \sigma_1 = e_2 + c_1 e_1, \quad \sigma_2 = e_4 + c_2 e_3. \quad (12)$$

where σ_1 and σ_2 are the sliding surfaces defined for pitch and yaw angle control, respectively. e_1 , e_2 , e_3 , and e_4 are the tracking errors of pitch angle, pitch angular velocity, yaw angle, and yaw angular velocity, respectively. c_1 and c_2 are positive design parameters. $e_1 = \theta_b - \theta_{bd}$, $e_2 = \dot{\theta}_b - \dot{\theta}_{bd}$, $e_3 = \theta_y - \theta_{yd}$, $e_4 = \dot{\theta}_y - \dot{\theta}_{yd}$. θ_{bd} , $\dot{\theta}_{bd}$, θ_{yd} , and $\dot{\theta}_{yd}$ are the desired values of pitch angle, pitch angular velocity, yaw angle, and yaw angular velocity, respectively. From Equation (12), we have

$$\begin{aligned} \dot{\sigma}_1 &= \dot{e}_2 + c_1 \dot{e}_1 = (\ddot{\theta}_b - \ddot{\theta}_{bd}) + c_1 \dot{e}_2, \\ \dot{\sigma}_2 &= \dot{e}_4 + c_2 \dot{e}_3 = (\ddot{\theta}_y - \ddot{\theta}_{yd}) + c_2 \dot{e}_4. \quad (13) \end{aligned}$$

According to the structure of SOSMC, we have [26]

$$\dot{\sigma}_1 = u_1 + h_1, \quad \dot{\sigma}_2 = u_2 + h_2. \quad (14)$$

where u_1 and u_2 are the equivalent control inputs. h_1 and h_2 are the disturbances. Comparing Equation (8), Equation (13), and Equation (14), for conventional method we have

$$\begin{cases} u_1 = A_{c1} + \hat{M}_{c31}^{-1} \tau_r + \hat{M}_{c32}^{-1} \tau_l - \ddot{\theta}_{bd} + c_1 e_2, & h_1 = B_{c1}, \\ u_2 = \frac{r}{d} [A_{c2} + (\hat{M}_{c11}^{-1} - \hat{M}_{c21}^{-1}) \tau_r + (\hat{M}_{c12}^{-1} - \hat{M}_{c22}^{-1}) \tau_l] & (15) \\ -\ddot{\theta}_{yd} + c_2 e_4, & h_2 = \frac{r}{d} B_{c2}. \end{cases}$$

To develop the SOSMC, K_{m1} and K_{M1} which are two positive constants are chosen as

$$0 \leq K_{m1} \leq 1 \leq K_{M1}$$

There exists two positive constants q_1 and U_{M1} which are selected as

$$|h_1| < q_1 U_{M1}, \quad 0 < q_1 < 1$$

Also, the positive constant value C_1 is chosen as

$$|\dot{h}_1| \leq C_1$$

Considering the assumptions above, the equivalent control input u_1 is defined as

$$\begin{aligned} u_1 &= -\lambda_1 |\sigma_1|^{0.5} \text{sign}(\sigma_1) + v_1, \\ \dot{v}_1 &= \begin{cases} -u_1, & |u_1| > U_{M1} \\ -\alpha_1 \text{sign}(\sigma_1), & |u_1| \leq U_{M1} \end{cases} \quad (16) \end{aligned}$$

where, λ_1 and α_1 are two positive constants. Selecting

$$\lambda_1 > \sqrt{\frac{2}{(K_{m1} \alpha_1 - C_1)} \frac{(K_{m1} \alpha_1 + C_1) K_{M1} (1 + q_1)}{K_{m1}^2 (1 - q_1)}}$$

and $\alpha_1 > C_1 / K_{m1}$, all tracking errors converge to zero in finite time. The stability proof of SOSMC can be found in [27].

Similar to u_1 , u_2 is defined as

$$\begin{aligned} u_2 &= -\lambda_2 |\sigma_2|^{0.5} \text{sign}(\sigma_2) + v_2, \\ \dot{v}_2 &= \begin{cases} -u_2, & |u_2| > U_{M2} \\ -\alpha_2 \text{sign}(\sigma_2), & |u_2| \leq U_{M2} \end{cases} \quad (17) \end{aligned}$$

From Equation (15) - Equation (17), the input torque of right and left wheels in conventional method can be obtained through

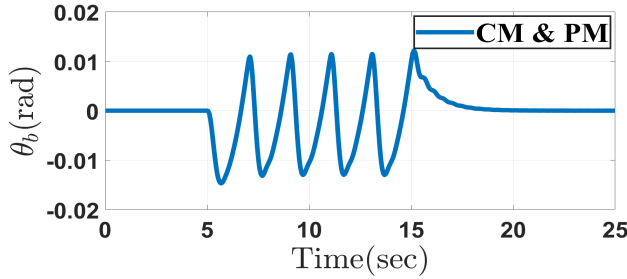
$$\begin{bmatrix} \tau_r \\ \tau_l \end{bmatrix} = \begin{bmatrix} \hat{M}_{c31}^{-1} & \hat{M}_{c32}^{-1} \\ (\hat{M}_{c11}^{-1} - \hat{M}_{c21}^{-1}) & (\hat{M}_{c12}^{-1} - \hat{M}_{c22}^{-1}) \end{bmatrix}^{-1} \begin{bmatrix} F_{c1} \\ F_{c2} \end{bmatrix} \quad (18)$$

where

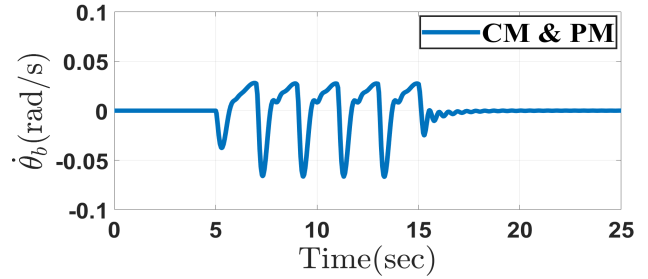
$$\begin{aligned} F_{c1} &= -A_{c1} + \ddot{\theta}_{bd} - c_1 e_2 - \lambda_1 |\sigma_1|^{0.5} \text{sign}(\sigma_1) + v_1, \\ F_{c2} &= -A_{c2} + \frac{d}{r} (\ddot{\theta}_{yd} - c_2 e_4 - \lambda_2 |\sigma_2|^{0.5} \text{sign}(\sigma_2) + v_2). \end{aligned}$$

TABLE 2. Physical parameters of the TWRW for simulation.

Property	m_w	\hat{m}_b	m_p	J_{w_y}	J_{w_z}	J_{b_x}	J_{b_y}	J_{b_z}	J_{p_x}	J_{p_y}	J_{p_z}	r	d	b	l	l'
Value	10	80	30	0.32	0.64	10.03	12.40	13.39	0.26	0.39	0.35	0.37	0.5	0.25	0.6	0.42
Unit	kg	kg	kg	kg.m ²	m	m	m	m	m							



(a): Pitch angle



(b): Pitch angular velocity

FIGURE 4. Response of the pitch angle and its angular velocity in the conventional method (CM) and the proposed method (PM).

B. PROPOSED METHOD

From Equation (11), Equation (13), and Equation (14), we have

$$\begin{cases} u_1 = A_{p1} + \hat{M}_{p31}^{-1}\tau_r + \hat{M}_{p32}^{-1}\tau_l + \hat{M}_{p34}^{-1}\tau_p - \ddot{\theta}_{bd} + c_1e_2, \\ h_1 = B_{p1}, \quad u_2 = \frac{r}{d}[A_{p2} + (\hat{M}_{p11}^{-1} - \hat{M}_{p21}^{-1})\tau_r \\ + (\hat{M}_{p12}^{-1} - \hat{M}_{p22}^{-1})\tau_l + (\hat{M}_{p14}^{-1} - \hat{M}_{p24}^{-1})\tau_p] - \ddot{\theta}_{yd} + c_2e_4, \\ h_2 = \frac{r}{d}B_{p2}. \end{cases} \quad (19)$$

To assist the wheels for stability and direction control, the input torque of added movable mechanism is defined as

$$\tau_p = \beta(\tau_r + \tau_l) \quad (20)$$

where $\beta > 0$. From Equation (16) - Equation (20), the input torque of right and left wheels and added mechanism can be obtained as

$$\begin{bmatrix} \tau_r \\ \tau_l \\ \tau_p \end{bmatrix} = \mathbf{W}^{-1} \begin{bmatrix} F_{p1} \\ F_{p1} \\ 0 \end{bmatrix} \quad (21)$$

where

$$\mathbf{W} = \begin{bmatrix} \hat{M}_{p31}^{-1} & \hat{M}_{p32}^{-1} & \hat{M}_{p34}^{-1} \\ (\hat{M}_{p11}^{-1} - \hat{M}_{p21}^{-1}) & (\hat{M}_{p12}^{-1} - \hat{M}_{p22}^{-1}) & (\hat{M}_{p14}^{-1} - \hat{M}_{p24}^{-1}) \\ \beta & \beta & -1 \end{bmatrix},$$

$$F_{p1} = -A_{p1} + \ddot{\theta}_{bd} - c_1e_2 - \lambda_1 |\sigma_1|^{0.5} \text{sign}(\sigma_1) + \nu_1,$$

$$F_{p2} = -A_{p2} + \frac{d}{r}(\ddot{\theta}_{yd} - c_2e_4 - \lambda_2 |\sigma_2|^{0.5} \text{sign}(\sigma_2) + \nu_2).$$

IV. SIMULATION RESULTS

To demonstrate through simulations the superiority of the proposed control method over conventional ones, the physical dimensions of the TWRW are chosen and listed in Table 2.

TABLE 3. Control parameter values.

Control parameter	c_1	λ_1	α_1	c_2	λ_2	α_2	β
Value	1	3	9.9	0.5	3	9.9	0.8

The values selected for the control parameters can be found in Table 3. The following initial conditions are assumed:

$$\theta_{b0} = \dot{\theta}_{b0} = \theta_{y0} = \dot{\theta}_{y0} = 0.$$

The following control objectives are set: $\theta_{bd} = 0, \dot{\theta}_{bd} = 0, \theta_{yd} = \frac{\pi}{2} \text{rad}, \dot{\theta}_{yd} = 0$.

The stability and direction control performances of the TWRW through conventional and the proposed methods are evaluated when the system is subject to the uncertainties of the mass of the body and its CoG which are respectively assumed as

$$\Delta m_b = 40 \text{ kg}, \quad \begin{cases} 0 \leq x_b \leq 5 \text{ cm} & 5 \leq t < 15 \\ x_b = 0 & \text{elsewhere} \end{cases}$$

Fig. 4 shows the response of pitch and its angular velocity. The results show that under the both controllers, system can keep its stability as the range of pitch angle and its rate is acceptable and after a period it converges to zero. It can be seen in Fig. 5 that the TWRW can reach its desired yaw angle and yaw angular velocity. The variation of pitch and yaw angle and their rates under the conventional and the proposed method are similar. The required input torque of right and left wheels can be seen in Fig. 6.

The results show that the required torque through the proposed method is lower than the conventional control approach. Similarly, the input power of wheels in the proposed approach is much lower than the conventional one (see Fig. 7). Fig. 8 depicts the input torque and power needed by the added mechanism which is lower than those needed by the right and left wheels.

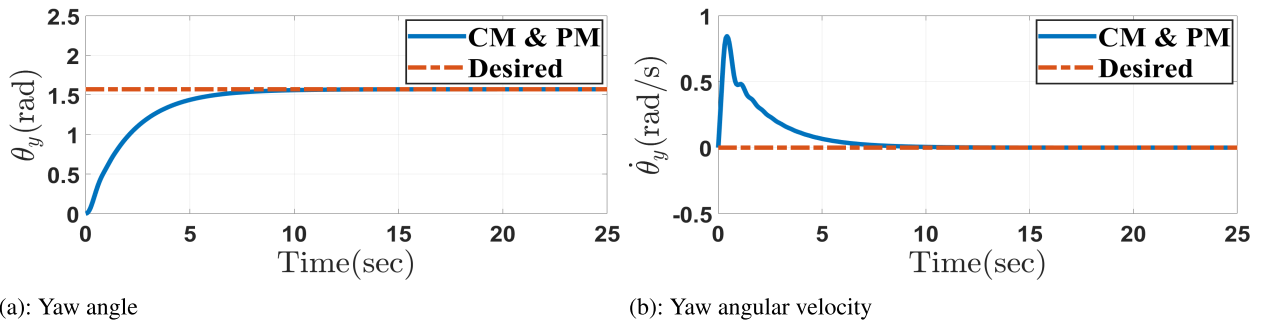


FIGURE 5. Response of the yaw angle and its angular velocity in the conventional method (CM) and the proposed method (PM).

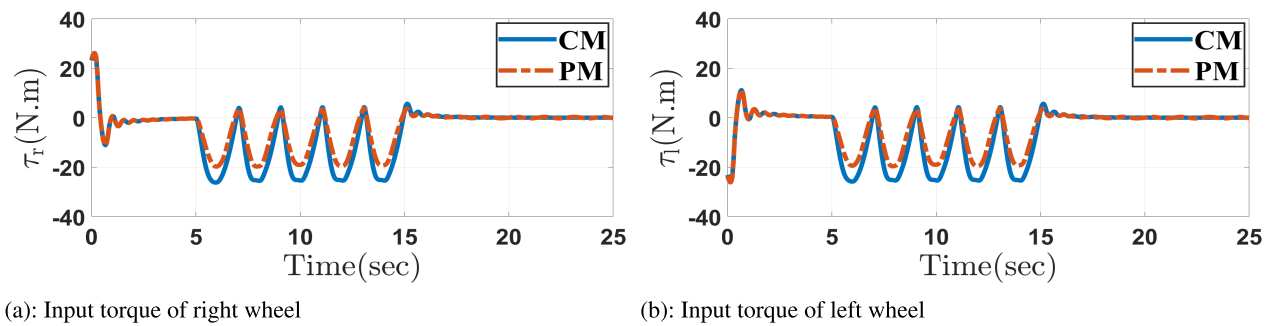


FIGURE 6. Input torque of right and left wheels in the conventional method (CM) and the proposed method (PM).

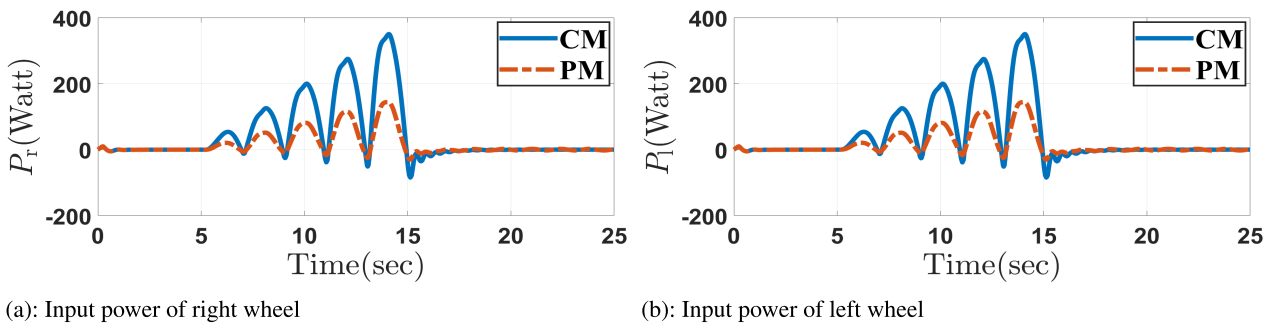


FIGURE 7. Input power of right and left wheels in the conventional method (CM) and the proposed method (PM).

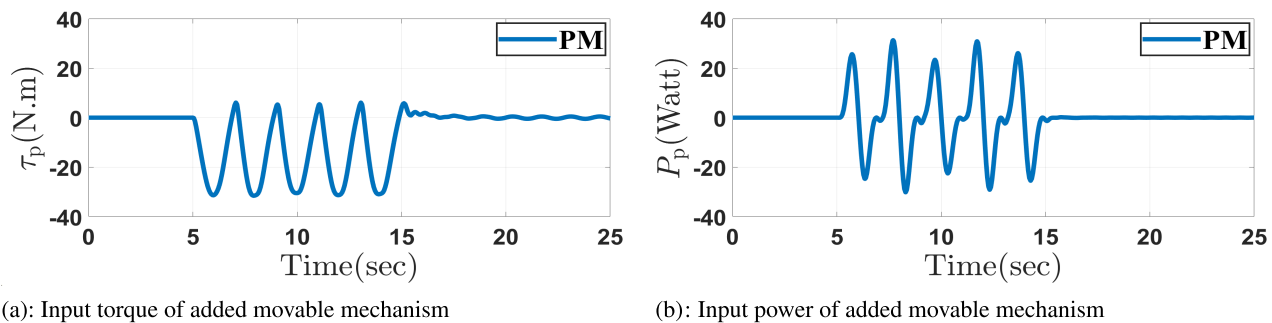


FIGURE 8. Input torque and power of the added movable mechanism in the proposed method (PM).

The energy consumption of the motors through the conventional and proposed approaches can be found in Table. 4. It can be seen that the energy consumption of right

and left wheels in the proposed approach are much lower than that of the conventional controller. The overall energy consumption including that for the added

TABLE 4. Energy consumption of motors in the conventional and the proposed method.

Energy consumption	Right wheel motor	Left wheel motor	added movable mechanism motor	overall
Conventional method	1256.10 J	1256.20 J		2512.30 J
Proposal method	482.66 J	483.11 J	119.76 J	1085.53 J

mechanism is also much lower than the conventional method.

V. CONCLUSION

In this paper, a novel approach is proposed for stability and direction control of a TWRW. A pendulum-like movable mechanism is added to the TWRW to assist the driving wheels to achieve the both control objectives. The Euler-Lagrange formulation is applied to establish the dynamic model of the system and a SOSMC which is robust against disturbances is developed for stability and direction control. The effectiveness of the proposed approach is simulated while considering disturbances caused by uncertainties of inertia parameter of the dynamic model and the rider’s motion. The simulation results demonstrate that in the proposed approach, the desired pitch and yaw angles of the TWRW desired for stability and direction control are achieved, while the input torque and power consumption for the control system are much lower than conventional methods.

APPENDIXES

APPENDIX A

DYNAMIC MODEL ELEMENTS OF THE CONVENTIONAL METHOD

The components of M_c and H_c are as below:

$$M_{c11} = M_{c22} = (m_w + \frac{1}{4}m_b)r^2 + J_{wz} + \frac{r^2}{d^2}[m_b l^2 \sin^2 \theta_b + 2J_{wy} + J_{bx} \sin^2 \theta_b + J_{by} \cos^2 \theta_b], \quad M_{c12} = \frac{1}{4}m_b r^2 - \frac{r^2}{d^2}[m_b l^2 \sin^2 \theta_b + 2J_{wy} + J_{bx} \sin^2 \theta_b + J_{by} \cos^2 \theta_b],$$

$$M_{c13} = M_{c23} = \frac{1}{2}m_b r l \cos \theta_b, \quad M_{c33} = m_b l^2 + J_{bz},$$

$$H_{c1} = \frac{r}{d} \dot{\theta}_y \dot{\theta}_b \sin 2\theta_b (m_b l^2 + J_{bx} - J_{by}) - \frac{1}{2} m_b r l \dot{\theta}_b^2 \sin \theta_b,$$

$$H_{c2} = -\frac{r}{d} \dot{\theta}_y \dot{\theta}_b \sin 2\theta_b (m_b l^2 + J_{bx} - J_{by}) - \frac{1}{2} m_b r l \dot{\theta}_b^2 \sin \theta_b,$$

$$H_{c3} = -\frac{1}{2} \dot{\theta}_y^2 \sin 2\theta_b (m_b l^2 + J_{bx} - J_{by}).$$

ΔM_c , ΔH_c , and R_c elements are

$$\Delta M_{11} = \Delta M_{22} = (\frac{1}{4} + \frac{l^2}{d^2} \sin^2 \theta_b) \Delta m_b r^2,$$

$$\Delta M_{12} = (\frac{1}{4} - \frac{l^2}{d^2} \sin^2 \theta_b) \Delta m_b r^2,$$

$$\Delta M_{13} = \Delta M_{23} = \frac{1}{2} \Delta m_b r l \cos \theta_b, \quad \Delta M_{33} = \Delta m_b l^2,$$

$$\Delta H_1 = (\frac{l}{d} \dot{\theta}_y \sin 2\theta_b - \frac{1}{2} \dot{\theta}_b \sin \theta_b) \Delta m_b r l \dot{\theta}_b,$$

$$\Delta H_2 = -(\frac{l}{d} \dot{\theta}_y \sin 2\theta_b + \frac{1}{2} \dot{\theta}_b \sin \theta_b) \Delta m_b r l \dot{\theta}_b,$$

$$\Delta H_3 = -\frac{1}{2} \dot{\theta}_y^2 \Delta m_b l^2 \sin 2\theta_b, \quad R_1 = \frac{r^2}{d^2} m_b x_b (x_b \cos^2 \theta_b + l \sin 2\theta_b) (\ddot{\theta}_r - \ddot{\theta}_l) - \frac{1}{2} m_b x_b r (\sin \theta_b \ddot{\theta}_b + \cos \theta_b \dot{\theta}_b^2)$$

$$- \frac{r}{d} m_b x_b \dot{\theta}_b \dot{\theta}_y (x_b \sin 2\theta_b - 2l \cos 2\theta_b),$$

$$R_2 = \frac{r^2}{d^2} m_b x_b (x_b \cos^2 \theta_b + l \sin 2\theta_b) (\dot{\theta}_l - \dot{\theta}_r)$$

$$- \frac{1}{2} m_b x_b r (\sin \theta_b \ddot{\theta}_b + \cos \theta_b \dot{\theta}_b^2) + \frac{r}{d} m_b x_b \dot{\theta}_b \dot{\theta}_y$$

$$(x_b \sin 2\theta_b - 2l \cos 2\theta_b), \quad R_3 = -\frac{1}{2} m_b x_b r$$

$$\sin \theta_b (\ddot{\theta}_r + \ddot{\theta}_l) + m_b x_b^2 \ddot{\theta}_b$$

$$+ \frac{1}{2} m_b x_b \dot{\theta}_y^2 (x_b \sin 2\theta_b - 2l \cos 2\theta_b) + m_b g x_b \cos \theta_b.$$

The definition of A_{c1} , B_{c1} , A_{c2} , and B_{c2} are as below

$$A_{c1} = -\hat{M}_{c31}^{-1} (H_{c1} + G_{c1}) - \hat{M}_{c32}^{-1} (H_{c2} + G_{c2}) - \hat{M}_{c33}^{-1} (H_{c3} + G_{c3}), \quad B_{c1} = -\hat{M}_{c31}^{-1} (D_{c1} + R_{c1}) - \hat{M}_{c32}^{-1} (D_{c2} + R_{c2}) - \hat{M}_{c33}^{-1} (D_{c3} + R_{c3}),$$

$$A_{c2} = (\hat{M}_{c21}^{-1} - \hat{M}_{c11}^{-1}) (H_{c1} + G_{c1}) + (\hat{M}_{c22}^{-1} - \hat{M}_{c12}^{-1}) (H_{c2} + G_{c2}) + (\hat{M}_{c23}^{-1} - \hat{M}_{c13}^{-1}) (H_{c3} + G_{c3}),$$

$$B_{c2} = (\hat{M}_{c21}^{-1} - \hat{M}_{c11}^{-1}) (D_{c1} + R_{c1}) + (\hat{M}_{c22}^{-1} - \hat{M}_{c12}^{-1}) (D_{c2} + R_{c2}) + (\hat{M}_{c23}^{-1} - \hat{M}_{c13}^{-1}) (D_{c3} + R_{c3}).$$

APPENDIX B

DYNAMIC MODEL ELEMENTS OF PROPOSED METHOD

The components of M_p , H_p , and G_p are as below:

$$M_{p11} = M_{p22} = (m_w + \frac{1}{4}m_b + \frac{1}{4}m_p)r^2 + J_{wz} + \frac{r^2}{d^2}[m_b l^2 \sin^2 \theta_b + 2J_{wy} + J_{bx} \sin^2 \theta_b + J_{by} \cos^2 \theta_b + m_p b^2 \sin^2 \theta_b + m_p l'^2 \sin^2 (\theta_b + \theta_p) + J_{px} \sin^2 (\theta_b + \theta_p) + J_{py} \cos^2 (\theta_b + \theta_p) - 2m_p b l' \sin \theta_b \sin (\theta_b + \theta_p)],$$

$$M_{p12} = \frac{1}{4} (m_b + m_p) r^2 - \frac{r^2}{d^2} [m_b l^2 \sin^2 \theta_b + 2J_{wy} + J_{bx} \sin^2 \theta_b + J_{by} \cos^2 \theta_b + m_p b^2 \sin^2 \theta_b + m_p l'^2 \sin^2 (\theta_b + \theta_p) + J_{px} \sin^2 (\theta_b + \theta_p) + J_{py} \cos^2 (\theta_b + \theta_p) - 2m_p b l' \sin \theta_b \sin (\theta_b + \theta_p)],$$

$$M_{p13} = M_{p23} = \frac{1}{2} r \cos \theta_b (m_b l + m_p b)$$

$$\begin{aligned}
& -\frac{1}{2}m_p r l' \cos(\theta_b + \theta_p), \\
M_{p14} = M_{p24} = & -\frac{1}{2}m_p r l' \cos(\theta_b + \theta_p), \\
M_{p33} = & m_b l^2 + m_p(b^2 + l'^2) + J_{b_z} + J_{p_z} - 2m_p b l' \cos\theta_p, \\
M_{p34} = & m_p l'^2 - m_p b l' \cos\theta_p + J_{p_z}, \quad M_{p44} = m_p l'^2 + J_{p_z}, \\
H_{p1} = & \frac{r}{d} \dot{\theta}_y \dot{\theta}_b \sin 2\theta_b (m_b l^2 + J_{b_x} - J_{b_y}) - \frac{1}{2} r \dot{\theta}_b^2 \sin\theta_b (m_b l \\
& + m_p b) + \frac{1}{2} m_p r l' (\dot{\theta}_b + \dot{\theta}_p)^2 \sin(\theta_b + \theta_p) \\
& + \frac{r}{d} m_p \dot{\theta}_y [b^2 \dot{\theta}_b \sin 2\theta_b + l'^2 (\dot{\theta}_b + \dot{\theta}_p) \sin(2\theta_b + 2\theta_p) \\
& - 2b l' \dot{\theta}_b \sin(2\theta_b + \theta_p) - 2l' b \dot{\theta}_p \sin\theta_b \cos(\theta_b + \theta_p)] \\
& + \frac{r}{d} \dot{\theta}_y (\dot{\theta}_b + \dot{\theta}_p) (J_{p_x} - J_{p_y}) \sin(2\theta_b + 2\theta_p), \\
H_{p2} = & -\frac{r}{d} \dot{\theta}_y \dot{\theta}_b \sin 2\theta_b (m_b l^2 + J_{b_x} - J_{b_y}) \\
& - \frac{1}{2} r \dot{\theta}_b^2 \sin\theta_b (m_b l + m_p b) \\
& + \frac{1}{2} m_p r l' (\dot{\theta}_b + \dot{\theta}_p)^2 \sin(\theta_b + \theta_p) - \frac{r}{d} m_p \dot{\theta}_y [b^2 \dot{\theta}_b \sin 2\theta_b \\
& + l'^2 (\dot{\theta}_b + \dot{\theta}_p) \sin(2\theta_b + 2\theta_p) - 2b l' \dot{\theta}_b \sin(2\theta_b + \theta_p) \\
& - 2b l' \dot{\theta}_p \sin\theta_b \cos(\theta_b + \theta_p)] \\
& - \frac{r}{d} \dot{\theta}_y (\dot{\theta}_b + \dot{\theta}_p) (J_{p_x} - J_{p_y}) \sin(2\theta_b + 2\theta_p), \\
H_{p3} = & -\frac{1}{2} \dot{\theta}_y^2 \sin 2\theta_b (m_b l^2 + J_{b_x} - J_{b_y}) \\
& + m_p b l' [(\dot{\theta}_p^2 + 2\dot{\theta}_b \dot{\theta}_p) \sin\theta_p] - \frac{1}{2} m_p \dot{\theta}_y^2 b^2 \sin 2\theta_b \\
& - \frac{1}{2} \dot{\theta}_y^2 [\sin(2\theta_b + 2\theta_p) (m_p l'^2 - 2m_p b l' + J_{p_x} - J_{p_y})], \\
G_{p3} = & -(m_b l + m_p b) g \sin\theta_b + m_p g l' \sin(\theta_b + \theta_p), \\
G_{p4} = & m_p g l' \sin(\theta_b + \theta_p).
\end{aligned}$$

The definition of A_{p1} , B_{p1} , A_{p2} , and B_{p2} are as below

$$\begin{aligned}
A_{p1} = & -\hat{M}_{p31}^{-1}(H_{p1} + G_{p1}) - \hat{M}_{p32}^{-1}(H_{p2} + G_{p2}) \\
& - \hat{M}_{p33}^{-1}(H_{p3} + G_{p3}) - \hat{M}_{p34}^{-1}(H_{p4} + G_{p4}), \\
B_{p1} = & -\hat{M}_{p31}^{-1}(D_{p1} + R_{p1}) - \hat{M}_{p32}^{-1}(D_{p2} + R_{p2}) \\
& - \hat{M}_{p33}^{-1}(D_{p3} + R_{p3}) - \hat{M}_{p34}^{-1}(D_{p4} + R_{p4}), \\
A_{p2} = & (\hat{M}_{p21}^{-1} - \hat{M}_{p11}^{-1})(H_{p1} + G_{p1}) \\
& + (\hat{M}_{p22}^{-1} - \hat{M}_{p12}^{-1})(H_{p2} + G_{p2}) + (\hat{M}_{p23}^{-1} - \hat{M}_{p13}^{-1}) \\
& (H_{p3} + G_{p3}) + (\hat{M}_{p24}^{-1} - \hat{M}_{p14}^{-1})(H_{p4} + G_{p4}), \\
B_{p2} = & (\hat{M}_{p21}^{-1} - \hat{M}_{p11}^{-1})(D_{p1} + R_{p1}) \\
& + (\hat{M}_{p22}^{-1} - \hat{M}_{p12}^{-1})(D_{p2} + R_{p2}) + (\hat{M}_{p23}^{-1} - \hat{M}_{p13}^{-1}) \\
& (D_{p3} + R_{p3}) + (\hat{M}_{p24}^{-1} - \hat{M}_{p14}^{-1})(D_{p4} + R_{p4}).
\end{aligned}$$

ACKNOWLEDGMENT

The authors would like to acknowledge Dr. Behrooz Lotfi and Simon Hartley for their advice and guidance.

REFERENCES

- [1] C. De La Cruz, T. F. Bastos, and R. Carelli, "Adaptive motion control law of a robotic wheelchair," *Control Eng. Pract.*, vol. 19, no. 2, pp. 113–125, Feb. 2011.
- [2] S. Oh and Y. Hori, "Disturbance attenuation control for power-assist wheelchair operation on slopes," *IEEE Trans. Control Syst. Technol.*, vol. 22, no. 3, pp. 828–837, May 2014.
- [3] S. Tashiro and T. Murakami, "Power-assist control of an electric wheelchair considering step passage," in *Proc. IEEE/ASME Int. Conf. Adv. Intell. Mechatronics*, Sep. 2007, pp. 1–6.
- [4] A. Dinale, K. Hirata, M. Zoppi, and T. Murakami, "Parameter design of disturbance observer for a robust control of two-wheeled wheelchair system," *J. Intell. Robotic Syst.*, vol. 77, no. 1, pp. 135–148, Oct. 2014.
- [5] Z. Li and C. Yang, "Neural-adaptive output feedback control of a class of transportation vehicles based on wheeled inverted pendulum models," *IEEE Trans. Control Syst. Technol.*, vol. 20, no. 6, pp. 1583–1591, Nov. 2012.
- [6] C.-H. Chiu, "Adaptive fuzzy control strategy for a single-wheel transportation vehicle," *IEEE Access*, vol. 7, pp. 113272–113283, 2019.
- [7] J. Huang, T. Zhang, Y. Fan, and J.-Q. Sun, "Control of rotary inverted pendulum using model-free backstepping technique," *IEEE Access*, vol. 7, pp. 96965–96973, 2019.
- [8] R. Cui, J. Guo, and Z. Mao, "Adaptive backstepping control of wheeled inverted pendulums models," *Nonlinear Dyn.*, vol. 79, no. 1, pp. 501–511, Sep. 2014.
- [9] A. Maddahi and A. H. Shamekhi, "Controller design for two-wheeled self-balancing vehicles using feedback linearisation technique," *Int. J. Vehicle Syst. Model. Test.*, vol. 8, no. 1, pp. 38–54, 2013.
- [10] K. Hirata and T. Murakami, "Stability analysis of disturbance observer based controllers for two-wheel wheelchair systems," *Adv. Robot.*, vol. 28, no. 7, pp. 467–477, Feb. 2014.
- [11] L. Vermeiren, A. Dequidt, T. M. Guerra, H. Rago-Tirmant, and M. Parent, "Modeling, control and experimental verification on a two-wheeled vehicle with free inclination: An urban transportation system," *Control Eng. Pract.*, vol. 19, no. 7, pp. 744–756, Jul. 2011.
- [12] S. Ahmad, N. H. Siddique, and M. O. Tokhi, "A modular fuzzy control approach for two-wheeled wheelchair," *J. Intell. Robotic Syst.*, vol. 64, nos. 3–4, pp. 401–426, Feb. 2011.
- [13] J. Huang, F. Ding, T. Fukuda, and T. Matsuno, "Modeling and velocity control for a novel narrow vehicle based on mobile wheeled inverted pendulum," *IEEE Trans. Control Syst. Technol.*, vol. 21, no. 5, pp. 1607–1617, Sep. 2013.
- [14] Y. Sago, Y. Noda, K. Kakahara, and K. Terashima, "Parallel two-wheel vehicle with underslung vehicle body," *Mech. Eng. J.*, vol. 1, no. 4, 2014, Art. no. DR0036.
- [15] M. Nikpour, L. Huang, A. M. Al-Jumaily, and B. Lotfi, "Stability control of mobile inverted pendulum through an added movable mechanism," in *Proc. 25th Int. Conf. Mechatronics Mach. Vis. Pract. (M2VIP)*, Nov. 2018, pp. 1–6.
- [16] A. Ghaffari, A. Shariati, and A. H. Shamekhi, "A modified dynamical formulation for two-wheeled self-balancing robots," *Nonlinear Dyn.*, vol. 83, nos. 1–2, pp. 217–230, Aug. 2015.
- [17] P. K. W. Abeygunawardhana, M. Defoort, and T. Murakami, "Self-sustaining control of two-wheel mobile manipulator using sliding mode control," in *Proc. 11th IEEE Int. Workshop Adv. Motion Control (AMC)*, Mar. 2010, pp. 792–797.
- [18] J. Huang, Z.-H. Guan, T. Matsuno, T. Fukuda, and K. Sekiyama, "Sliding-mode velocity control of mobile-wheeled inverted-pendulum systems," *IEEE Trans. Robot.*, vol. 26, no. 4, pp. 750–758, Aug. 2010.
- [19] M. Yue and X. Wei, "Dynamic balance and motion control for wheeled inverted pendulum vehicle via hierarchical sliding mode approach," *Proc. Inst. Mech. Eng., I, J. Syst. Control Eng.*, vol. 228, no. 6, pp. 351–358, Apr. 2014.
- [20] T. Elmokadem, M. Zribi, and K. Youcef-Toumi, "Control for dynamic positioning and way-point tracking of underactuated autonomous underwater vehicles using sliding mode control," *J. Intell. Robotic Syst.*, vol. 95, nos. 3–4, pp. 1113–1132, Apr. 2018.
- [21] R. Guruganesh, B. Bandyopadhyay, H. Arya, and G. K. Singh, "Design and hardware implementation of autopilot control laws for MAV using super twisting control," *J. Intell. Robotic Syst.*, vol. 90, nos. 3–4, pp. 455–471, Nov. 2017.
- [22] S. S. Rao and F. F. Yap, *Mechanical Vibrations*. vol. 4. Upper Saddle River, NJ, USA: Prentice-Hall, 2011.

- [23] N. Esmaili, A. Alfi, and H. Khosravi, "Balancing and trajectory tracking of two-wheeled mobile robot using backstepping sliding mode control: Design and experiments," *J. Intell. Robotic Syst.*, vol. 87, nos. 3–4, pp. 601–613, Jan. 2017.
- [24] M. G. Rodd, "Introduction to robotics: Mechanics and control," *Automatica*, vol. 23, no. 2, pp. 263–264, Mar. 1987.
- [25] D. S. Naidu, *Mechatronics: Electronic Control Systems in Mechanical Engineering*. London, U.K.: Pearson, 2003.
- [26] Y. Shtessel, C. Edwards, L. Fridman, and A. Levant, *Sliding Mode Control and Observation*. New York, NY, USA: Springer, 2014.
- [27] Z. Zhao, J. Yang, S. Li, Z. Zhang, and L. Guo, "Finite-time super-twisting sliding mode control for Mars entry trajectory tracking," *J. Franklin Inst.*, vol. 352, no. 11, pp. 5226–5248, Nov. 2015.



MOSTAFA NIKPOUR received the B.Sc. (Eng.) degree in mechanical engineering from the Quchan University of Technology, Iran, in 2013, and the M.Sc. (Eng.) degree (Hons.) in mechanical engineering from the Islamic Azad University of Mashhad, Iran, in 2016. He is currently pursuing the Ph.D. degree with the Auckland University of Technology, New Zealand. His research interests include robotics, dynamic modeling of nonlinear systems, and signal processing.



LOULIN HUANG (Member, IEEE) is currently an Associate Professor in mechatronics with the Auckland University of Technology (AUT). He had about 30 years' research experience in the areas of robotics, mechatronics, and control in his academic careers at the Huazhong University of Science and Technology, China, Singapore Polytechnic, Singapore, Massey University, New Zealand, and AUT. He has completed more than 30 industrial and government-funded projects and has about 100 publications.



AHMED M. AL-JUMAILY is currently a Professor of biomechanical engineering with the Institute of Biomedical Technologies, Auckland University of Technology, New Zealand. He has published more than 350 articles in international journals and conference proceedings in biomedical applications, system dynamics, and vibrations and control. He is a member of 11 international professional societies. He is the Editor-in-Chief of the *ASME Journal of Engineering and Science in Medical Diagnostics and Therapy* and the ASME monograph series—*Biomedical and Nanomedical Technologies*.

• • •